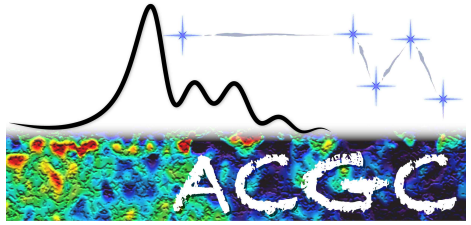

M31 & M33
the SF-HI Connection

T. Jarrett
(Cape Town)

ASTRON
19 March 2014

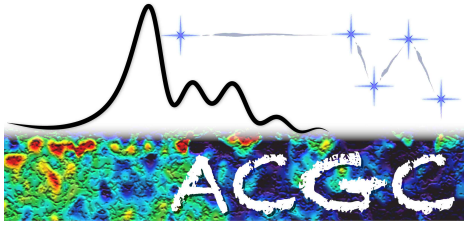

Exploring past to present star formation in Local Volume galaxies

T. Jarrett
E. Elson
P. Chauke
C. Carignan

LVHIS ⟺ WISE

Fuel to Fireworks

M83: PAH vs HI Reservoir

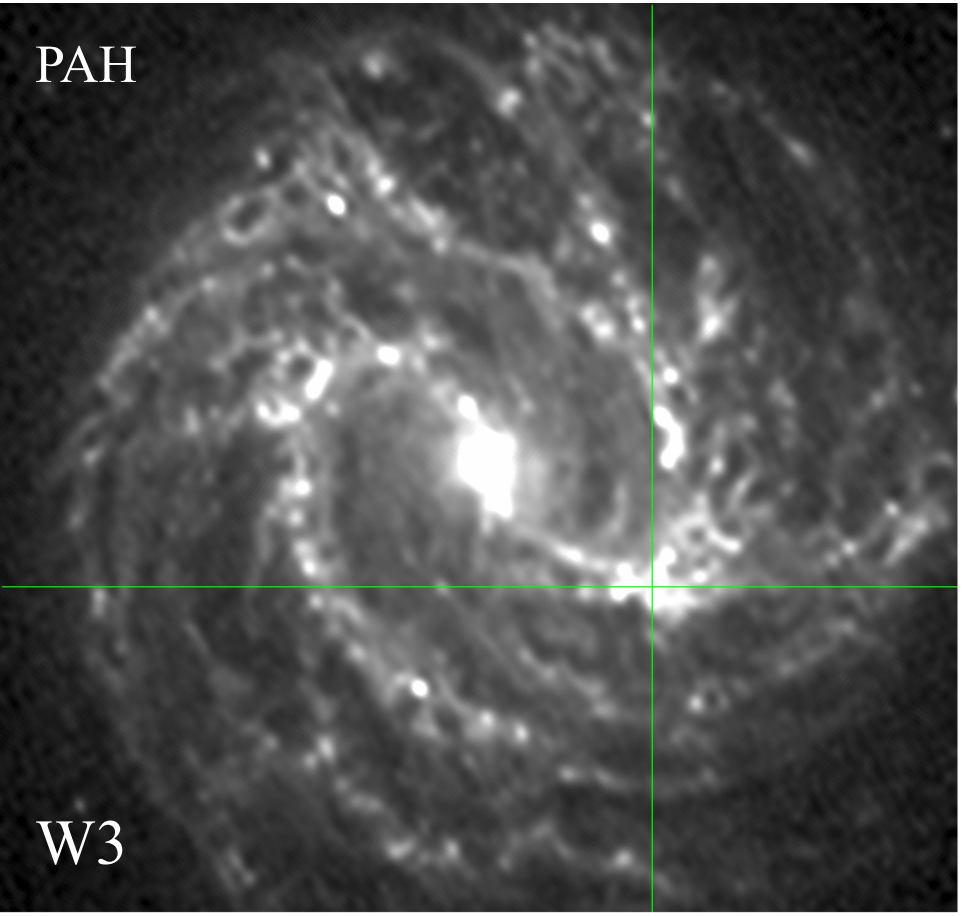

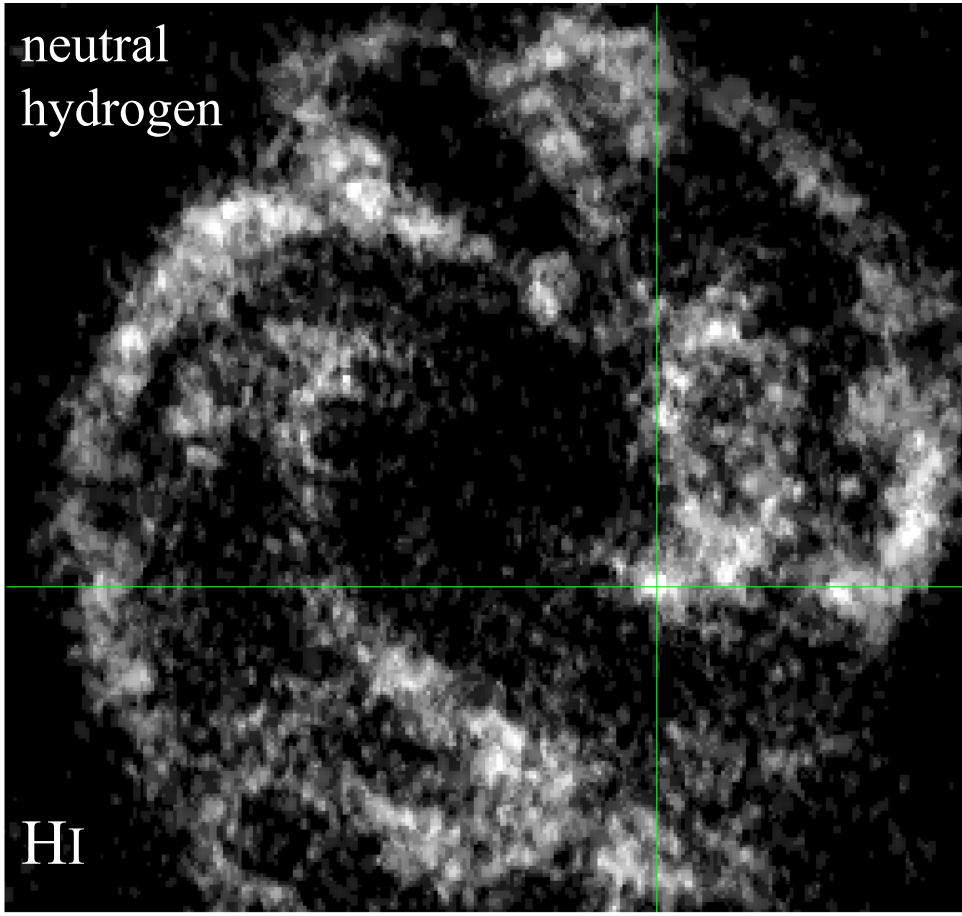

Jarrett et al. 2013

ATCA high-resolution
(Koribalski)

Andromeda

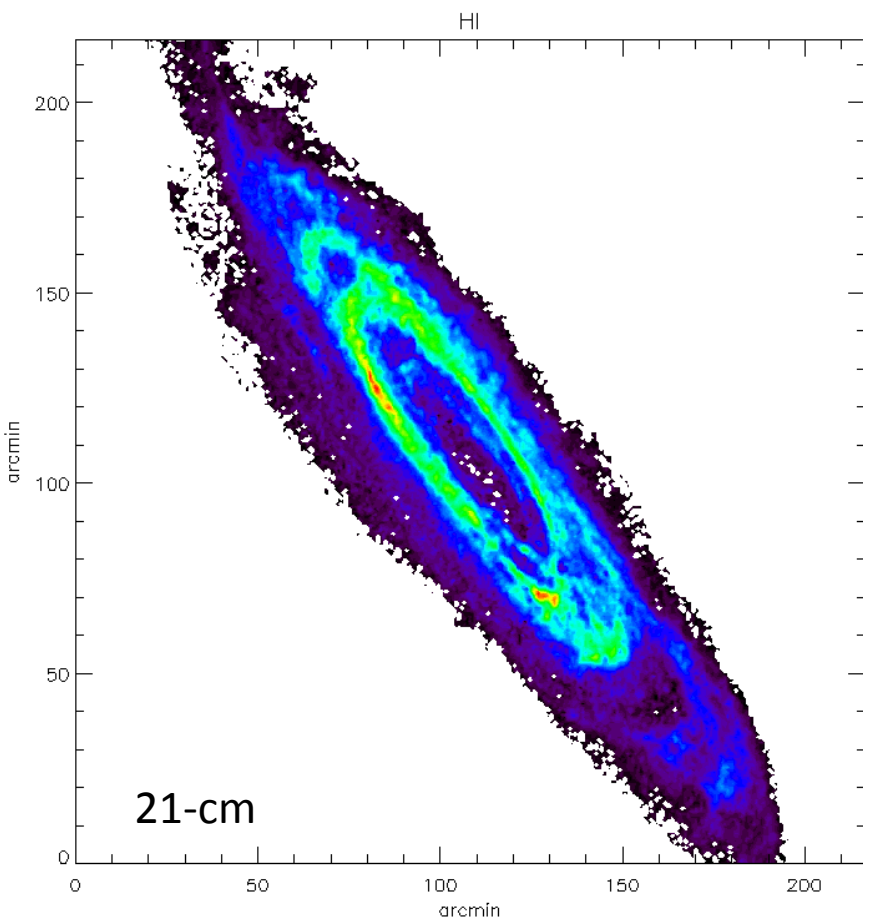

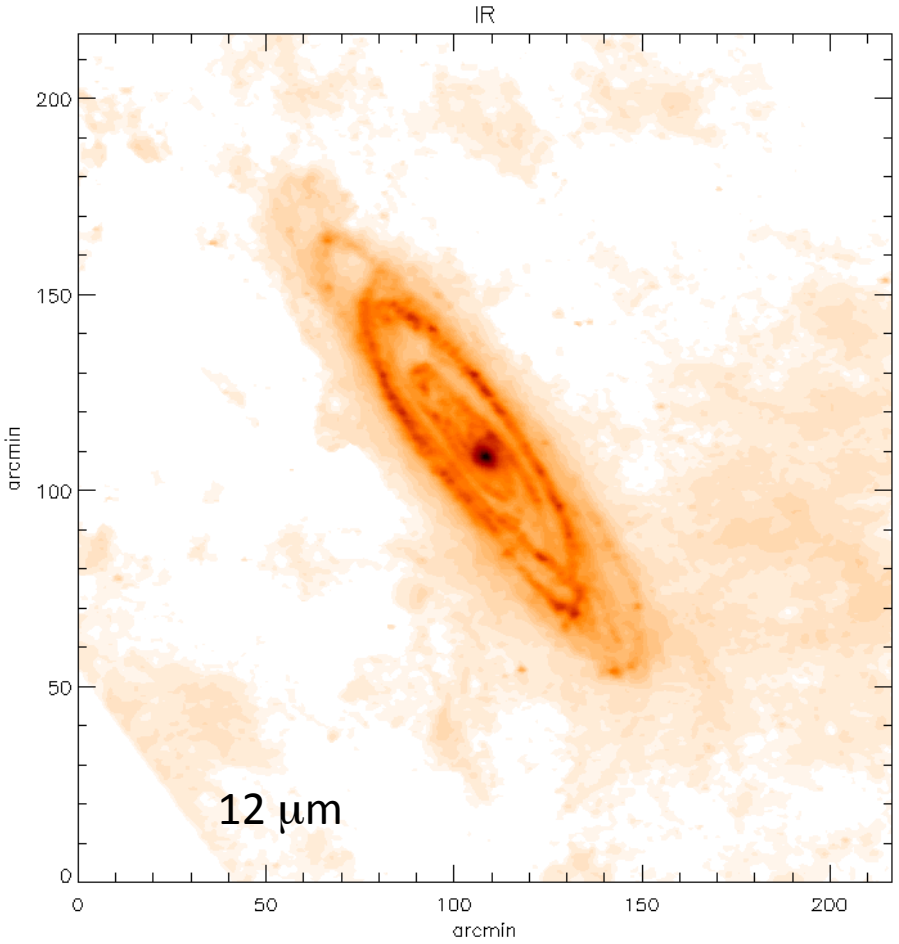

- Characterization of M31 mid-Infrared Imaging (masters thesis)
- Global Properties
- Detailed comparison with HI

mid-IR Mass/SF tracers

WISE

3.4, 4.5μm : host mass

12 μm: molecules

22 μm: warm dust

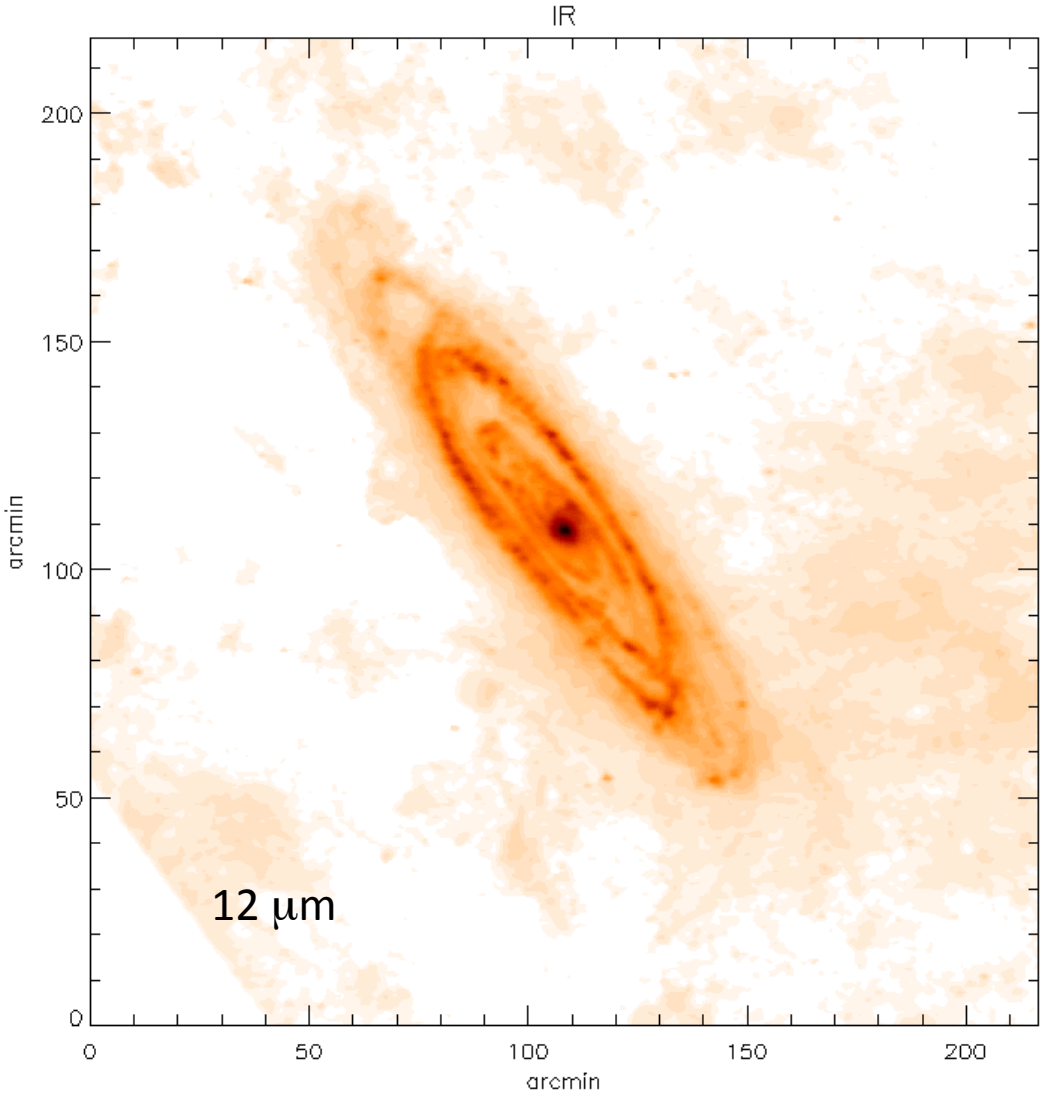

The Trouble with Andromeda

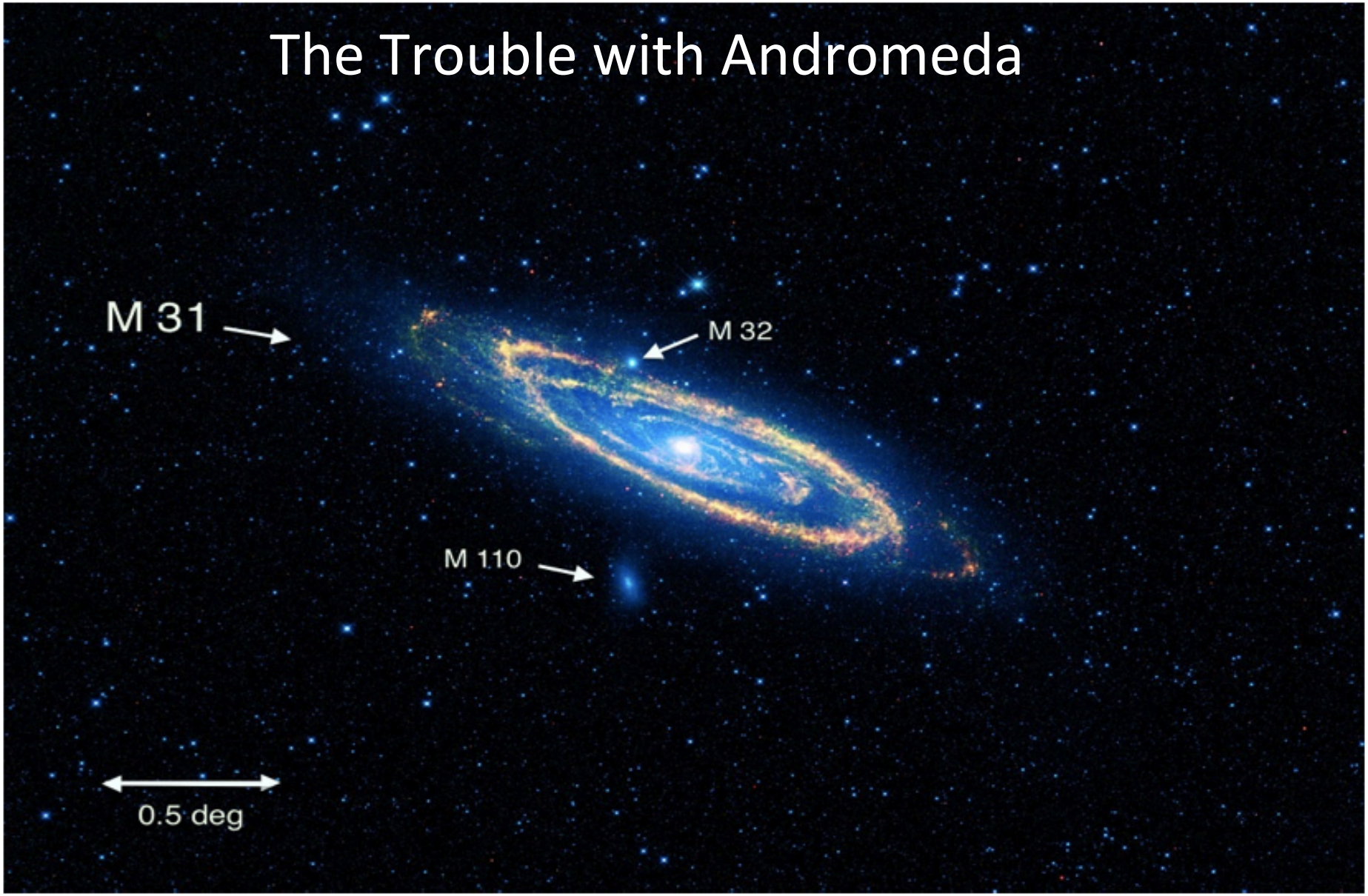

Figure 1.1: Combined WISE W1 (blue), W2 (green), and W3 (red) image of the M 31 region spanning 5°.

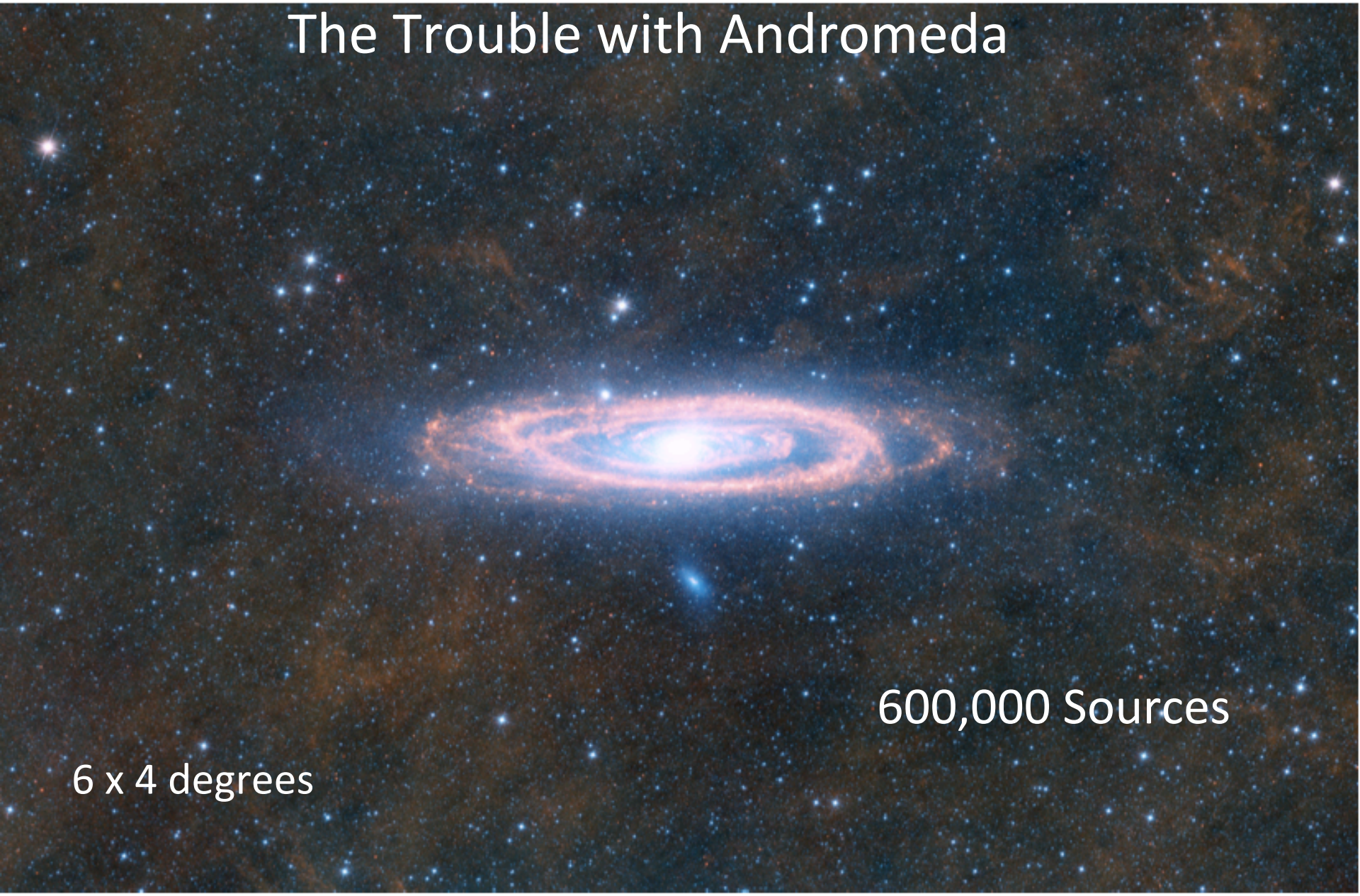
The Trouble with Andromeda
600,000 Sources
6 x 4 degrees

P. Chauke (2014)

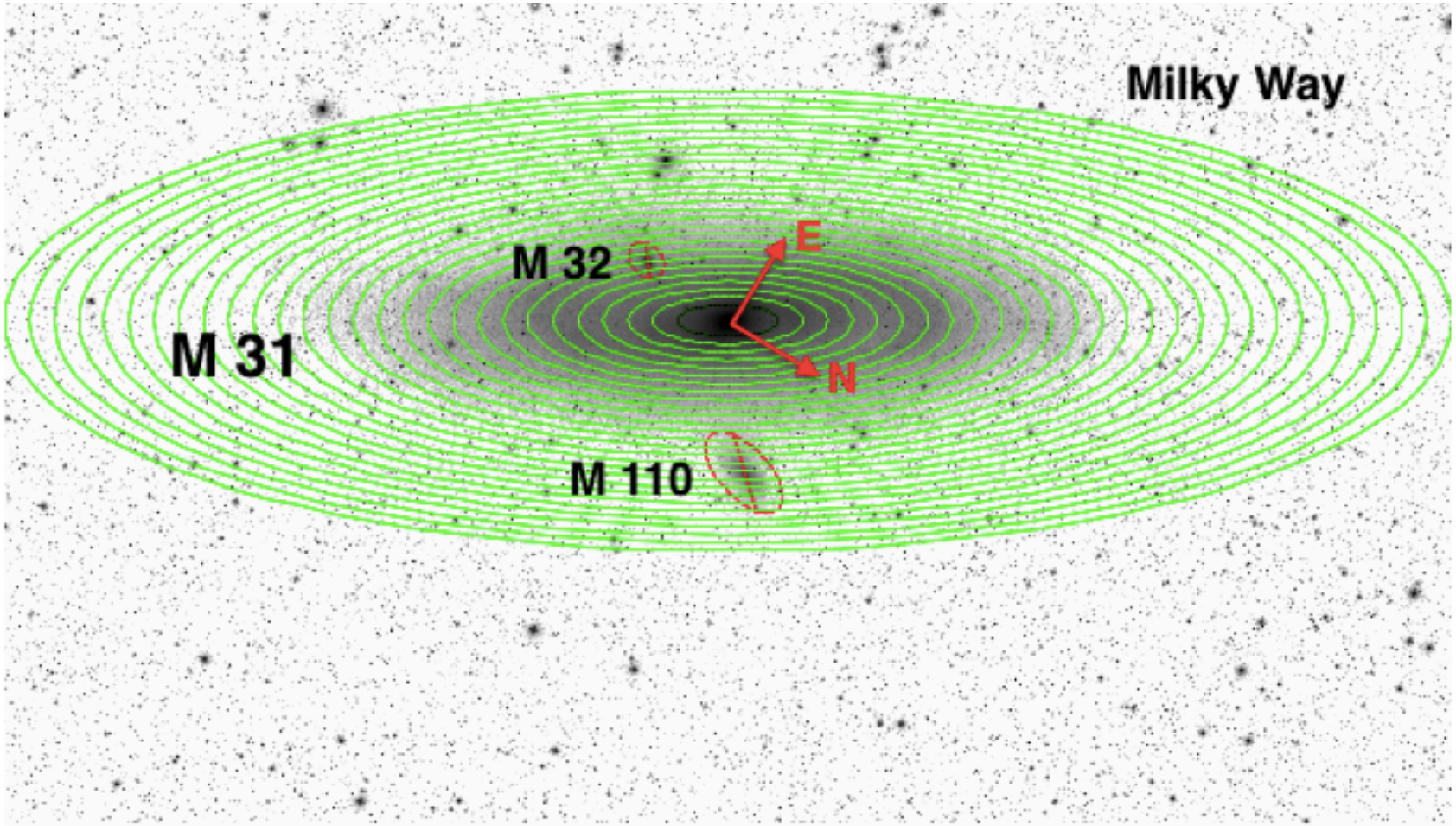

Source identification

- Milky Way stars
- M31 sources (stars, SF regions, GCs)
- satellites
- background galaxies

Assuming that the features are independent of each other, the probability that a source is of type C_i is

$$P(C_i|D_j, ..., D_n) = \sum_j^n w_j \times p(C_i|D_j) \tag{1.2}$$

where $w_j \in [0, 1]$ is the weight, the belief in the class C_i and $p(C_i|D_j)$ is the likelihood of the possibility of C_i with feature D_j. As one cannot be absolutely certain of the class of a source, each source is assigned a random number, $ran(u) \in [0, 1]$, which is then compared to the probability metric in (1.2), determining whether a source is of type C_1 or C_2.

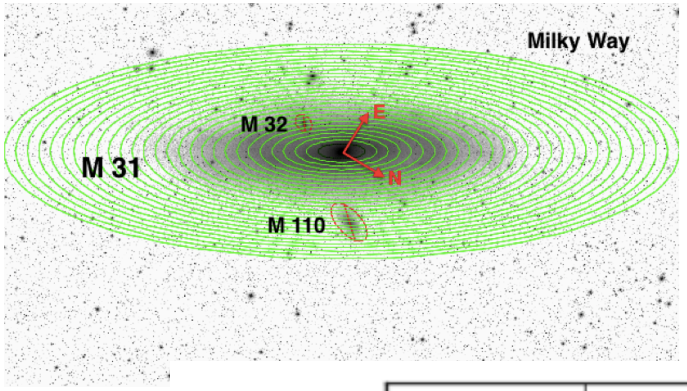

Proximity

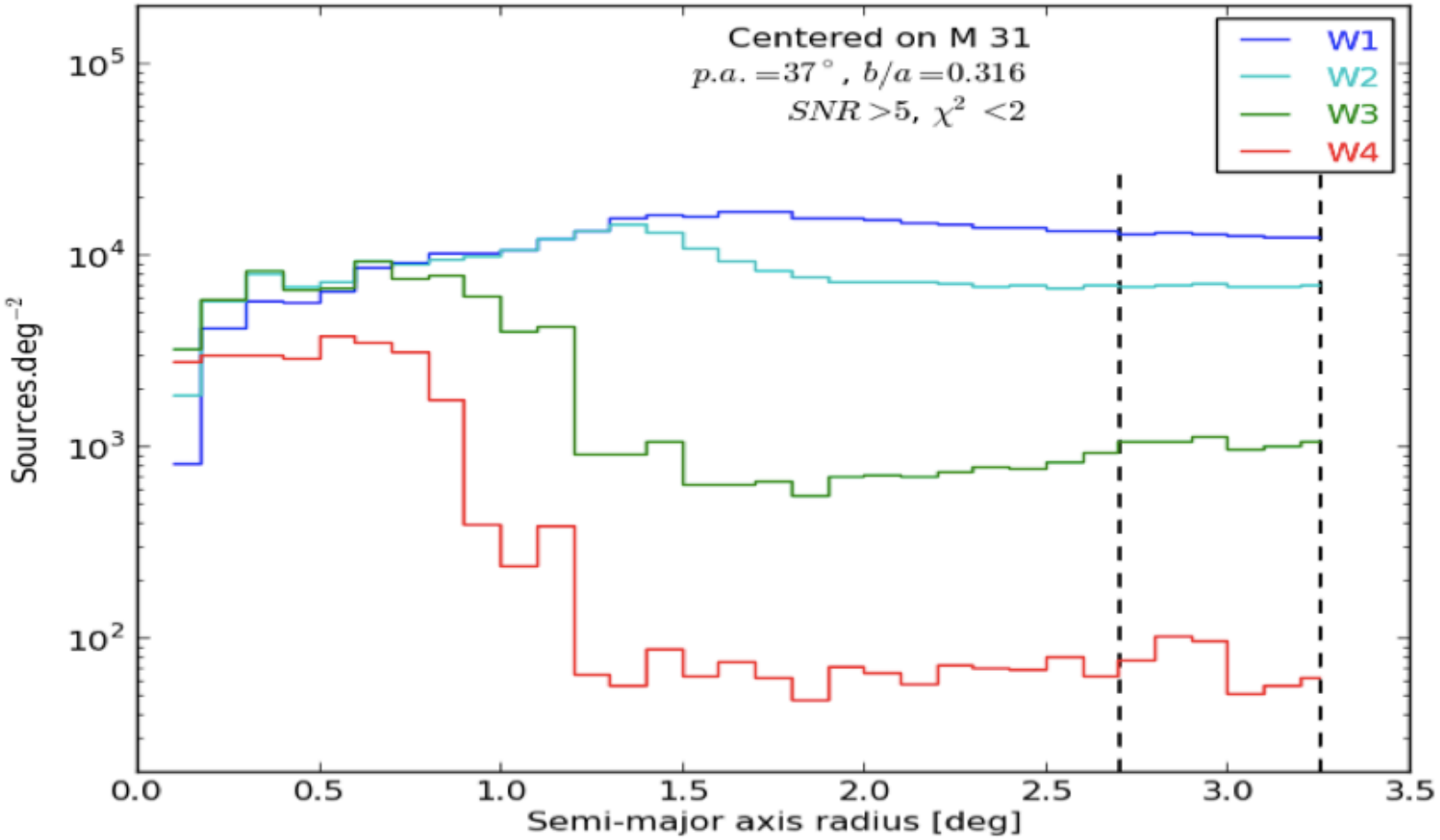

Figure 1.3: Mean axisymmetric W1, W2, W3 and W4 source counts as a function of radius.

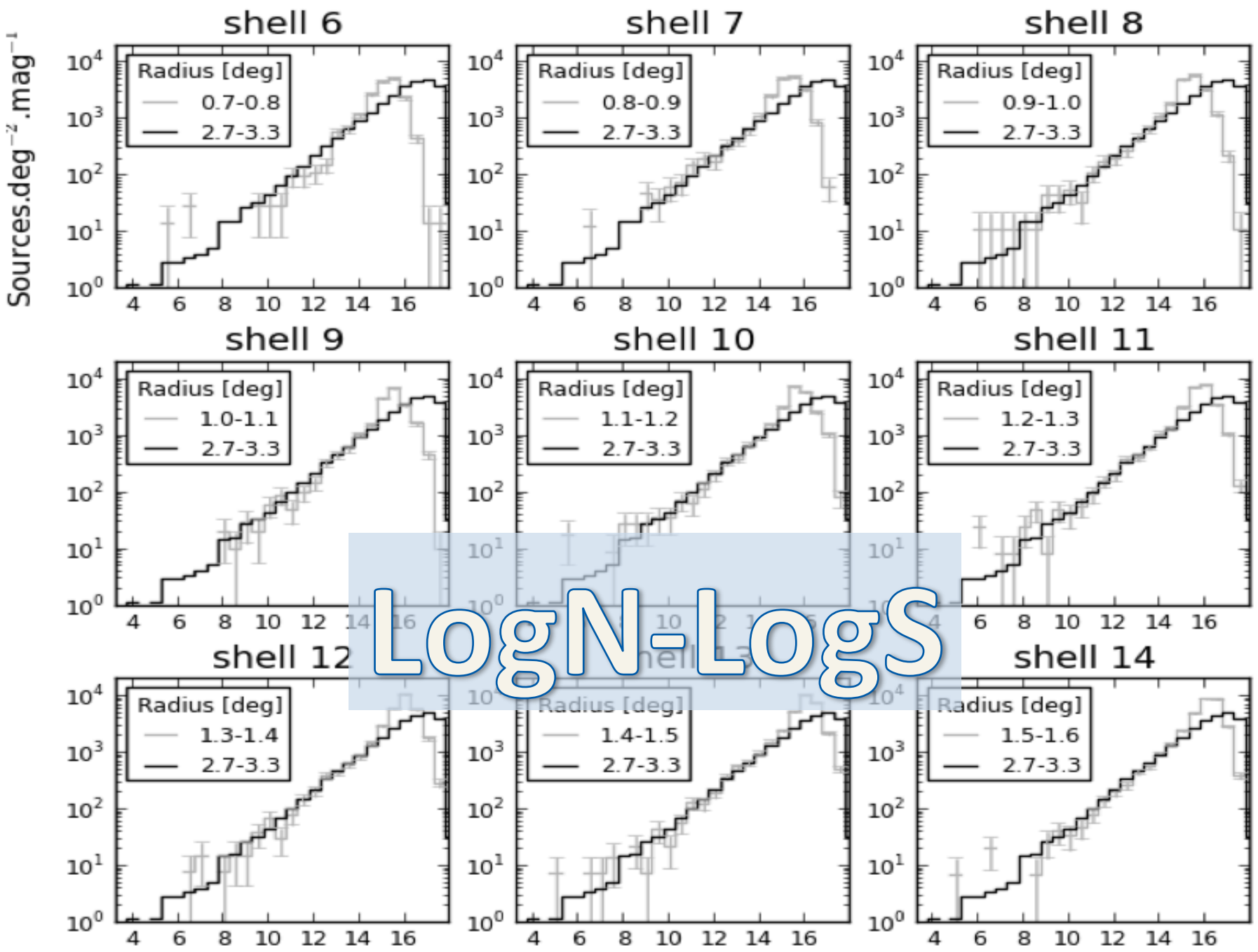
shell 6
Radius [deg]
0.7-0.8
2.7-3.3
shell 7
Radius [deg]
0.8-0.9
2.7-3.3
shell 8
Radius [deg]
0.9-1.0
2.7-3.3
shell 9
Radius [deg]
1.0-1.1
2.7-3.3
shell 10
Radius [deg]
1.1-1.2
2.7-3.3
shell 11
Radius [deg]
1.2-1.3
2.7-3.3
shell 12
Radius [deg]
1.3-1.4
2.7-3.3
Radius [deg]
1.4-1.5
2.7-3.3
shell 14
Radius [deg]
1.5-1.6
2.7-3.3
Sources.deg^{-2}.mag^{-1}
LogN-LogS

Colors

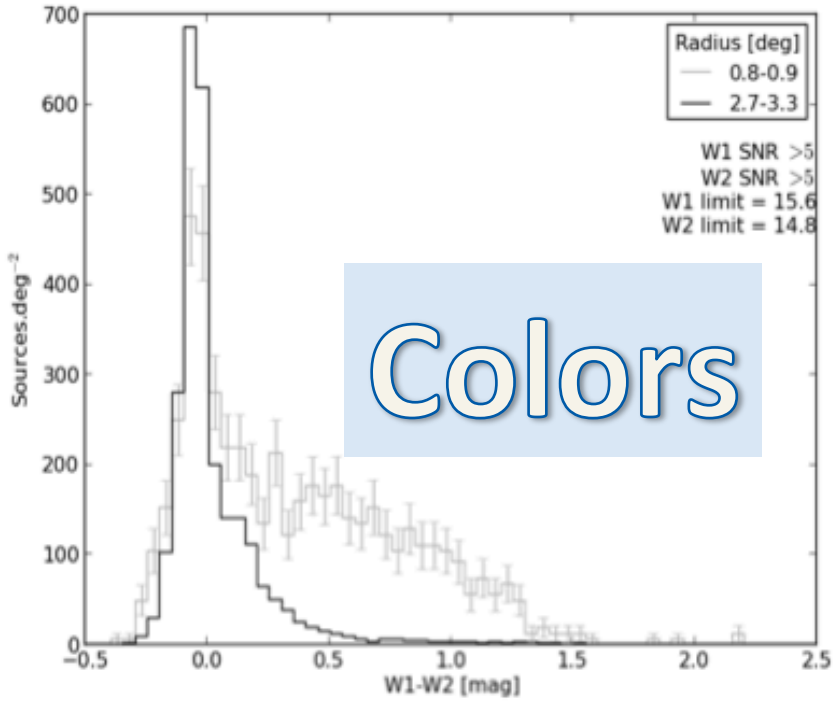
Radius [deg]
0.8-0.9
2.7-3.3
W1 SNR >5
W2 SNR >5
W1 limit = 15.6
W2 limit = 14.8
Sources.deg^{-2}
W1-W2 [mag]

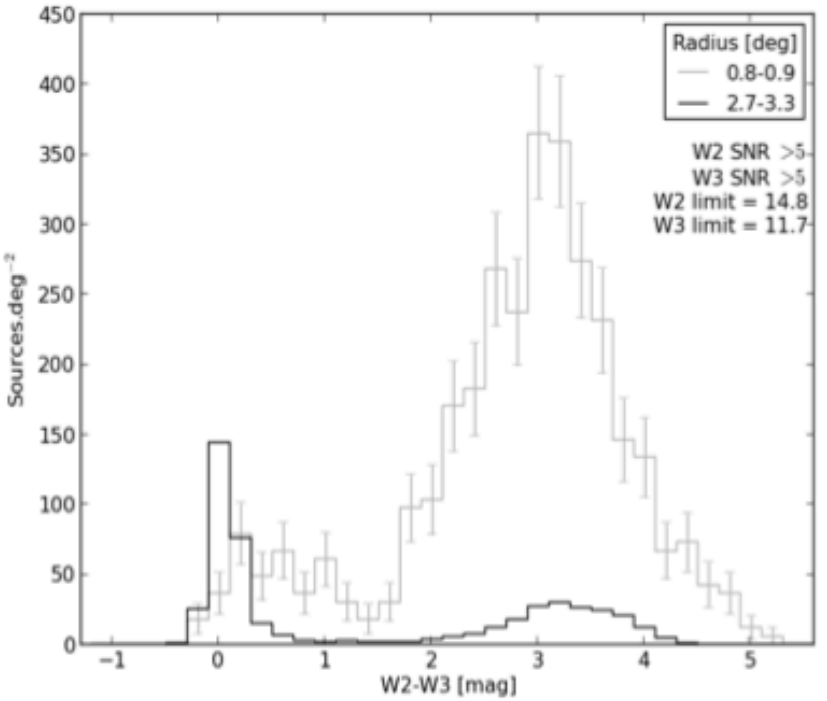
Radius [deg]
0.8-0.9
2.7-3.3
W2 SNR >5
W3 SNR >5
W2 limit = 14.8
W3 limit = 11.7
Sources.deg^{-2}
W2-W3 [mag]

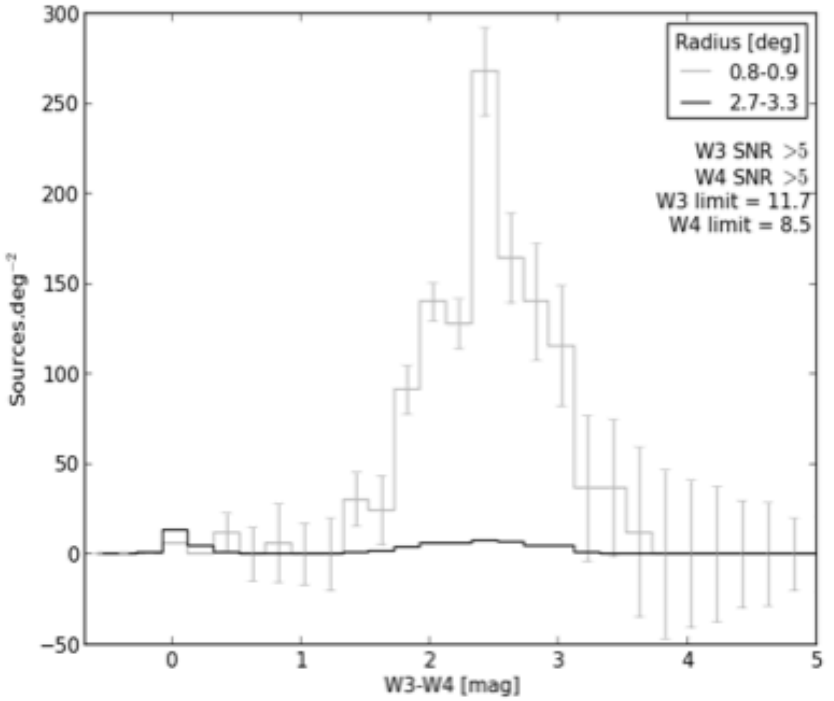
Radius [deg]
0.8-0.9
2.7-3.3
W3 SNR >5
W4 SNR >5
W3 limit = 11.7
W4 limit = 8.5
Sources.deg^{-2}
W3-W4 [mag]

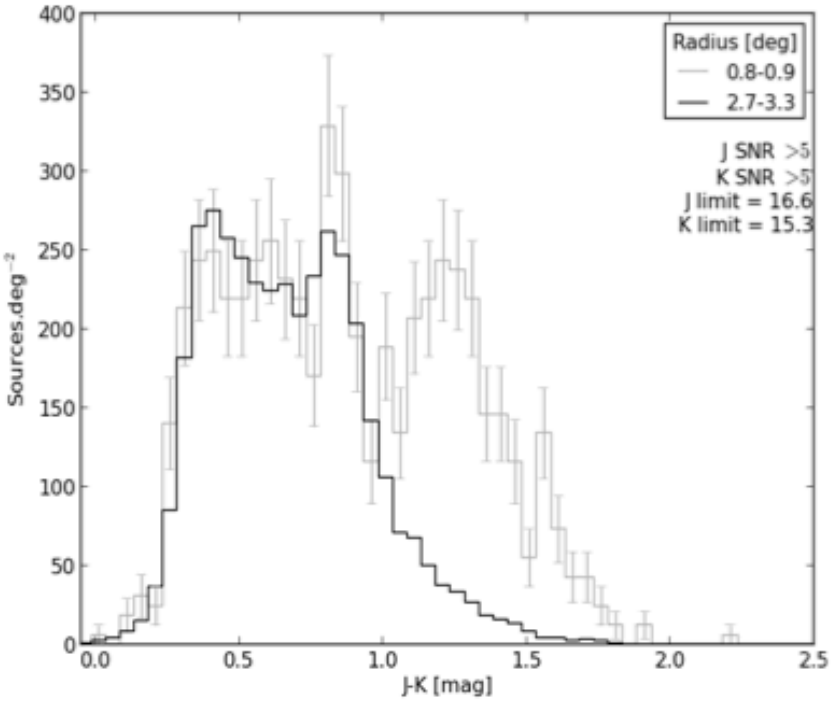
Radius [deg]
0.8-0.9
2.7-3.3
J SNR >5
K SNR >5
J limit = 16.6
K limit = 15.3
Sources.deg^{-2}
J-K [mag]

70% sources MW

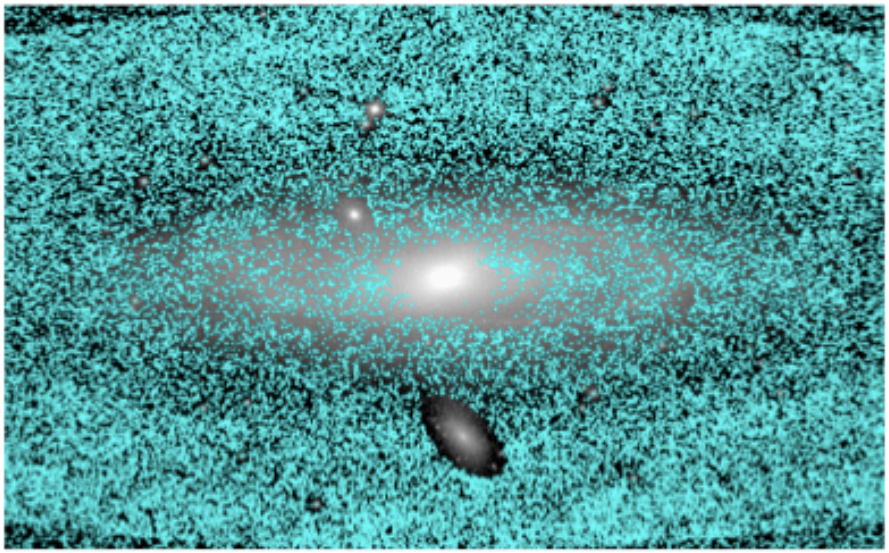

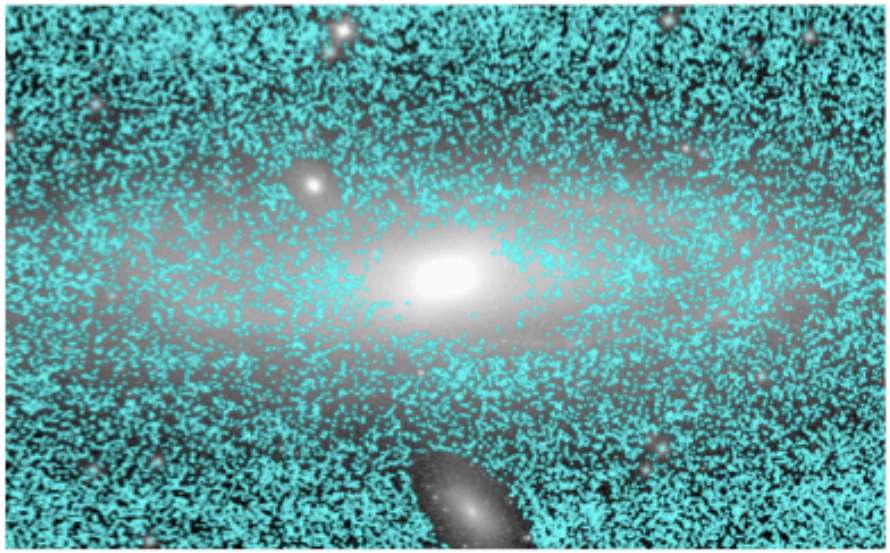

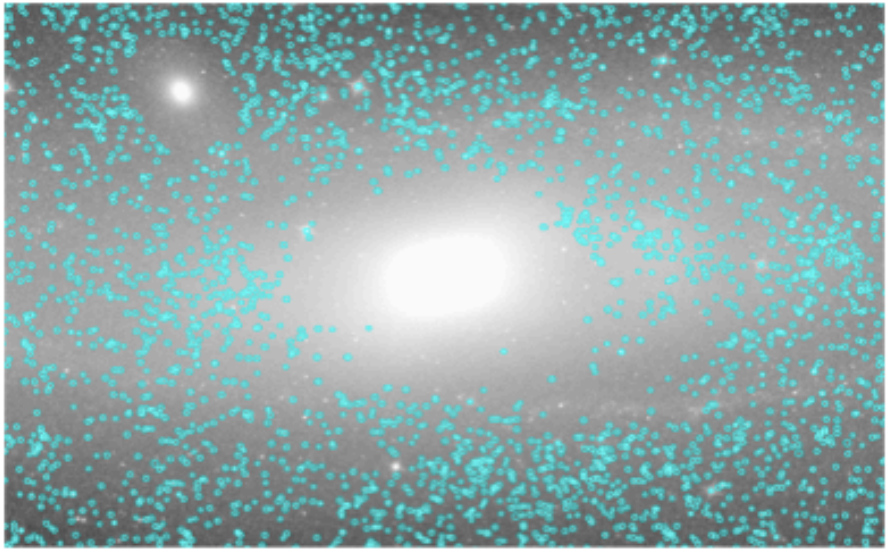

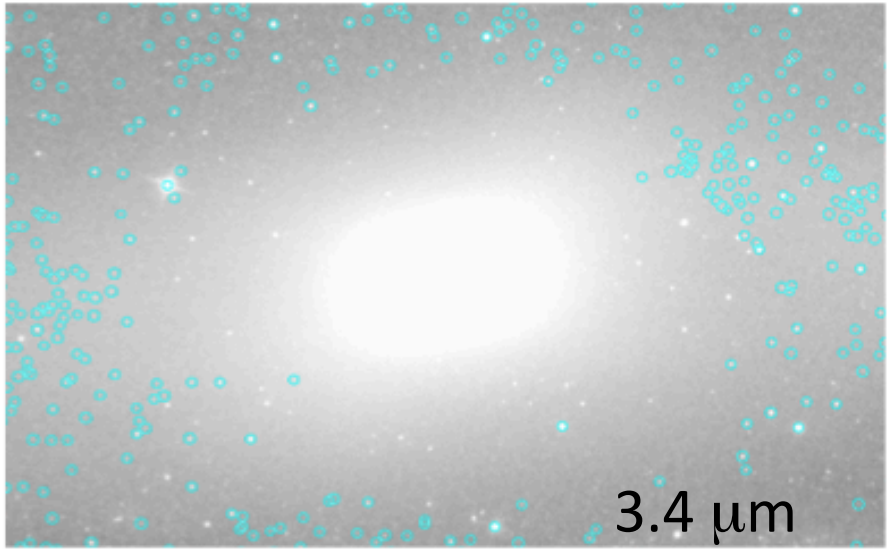

Global Measurements

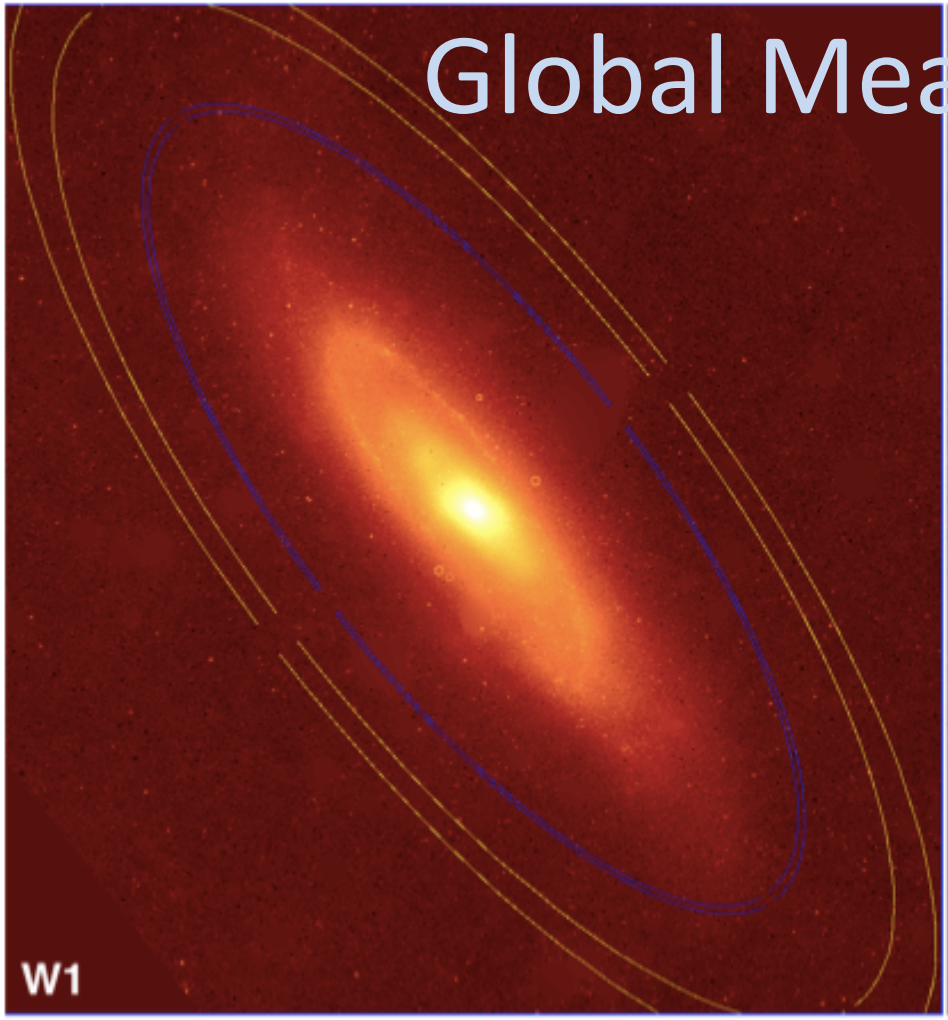

Table 1.1: Mid-IR isophotal-aperture Photometry.

Name	R.A. (°)	Decl. (°)	Axis Ratio	P.A. (°)	$R1_{iso}$ ($''$)	W1 (Jy)	W2 (Jy)	W3 (Jy)	W4 (Jy)
M 31	10.68479	41.26907	0.35	37.3	6686.1	285.336 ±2.994	151.769 ±1.594	175.543 ±1.842	142.705 ±1.544

Derived Parameters

Table 1.7: Stellar Mass

Name	$\log_{10} M_{stellar}/L_{W1}$	L_{W1} [a] $[L_\odot]$	$M_{stellar}$ $[M_\odot]$
M 31	-0.095	1.1×10^{11}	8.7×10^{10}
M 33	-0.173	9.0×10^{9}	6.1×10^{9}

massive

Notes. [a] The distances used to obtain the luminosities were 785 and 880 kpc for M 31 and M 33 respectively.

Table 1.8: IR and UV Global Star Formation Rates using Different Prescriptions.

Name		IR (12 μm)		IR (22 μm)		IR (24 μm)	FUV (0.15 μm)	NUV (0.23 μm)
		a	*b*	*a*	*b*	*c*	*d*	*e*
M 31	$\log(\nu L_\nu/L_\odot)$	8.937	8.937	8.525	8.525	8.459	8.802	8.986
	SFR $[M_\odot \mathrm{yr}^{-1}]$	0.4	0.7	0.3	0.5	0.2	0.1	0.2
M 33	$\log(\nu L_\nu/L_\odot)$	8.214	8.214	8.120	8.120	8.069	8.942	8.874
	SFR $[M_\odot \mathrm{yr}^{-1}]$	0.1	0.1	0.1	0.2	0.1	0.2	0.1

The 12 and 22 µm SFRs are derived using relations from both Jarrett et al. (2013) and Cluver et al. (2014)

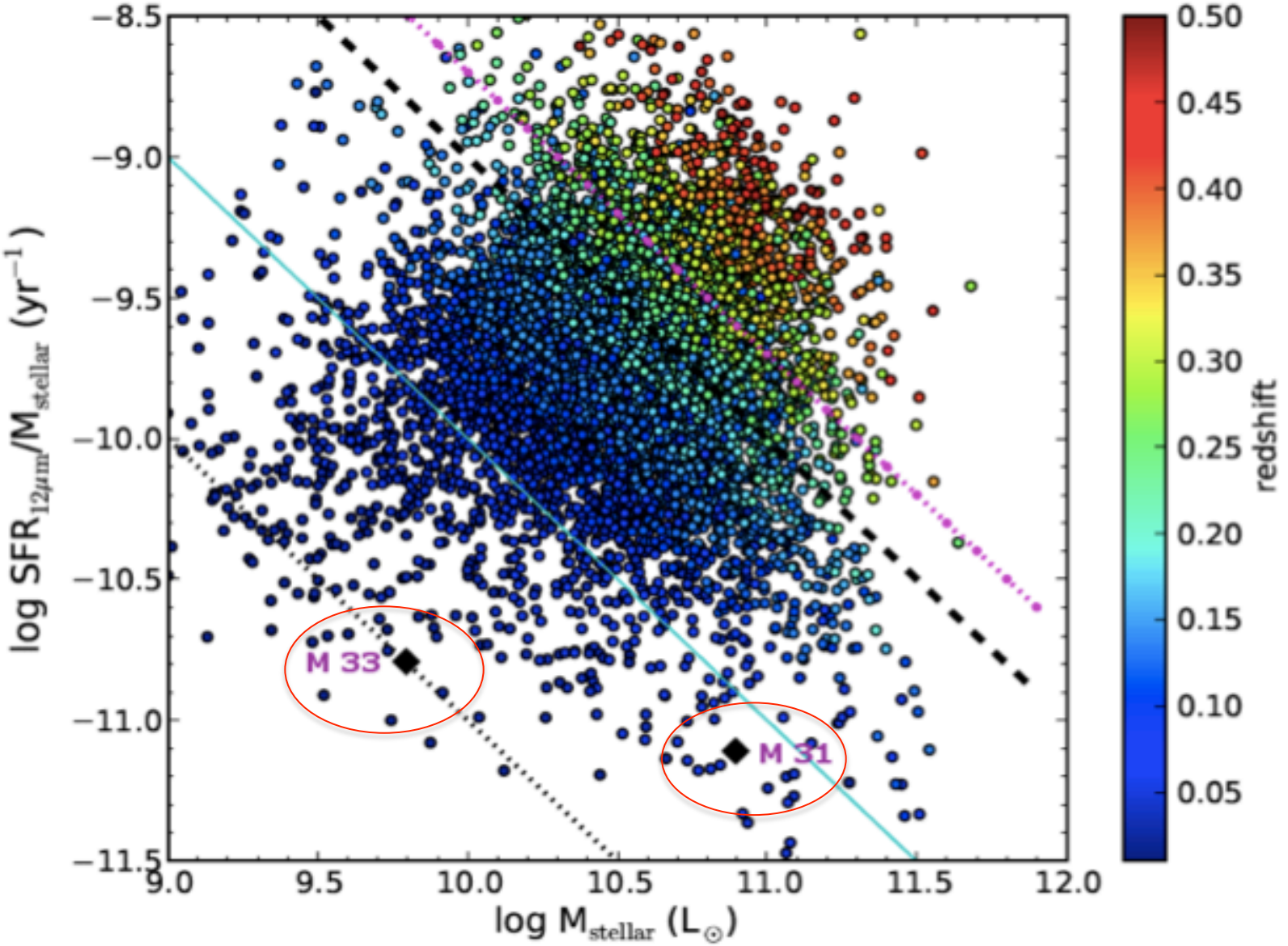

Figure 1.8: Specific star formation colour-coded with redshift derived by Cluver et al. (2014). The positions for M 31 and M 33 are over plotted in black for comparison. Lines of constant SFR (0.1, 1, 10 and 20 $M_\odot yr^{-1}$) are shown as dotted, solid, dashed and dash-dot lines, respectively.

Neutral Hydrogen

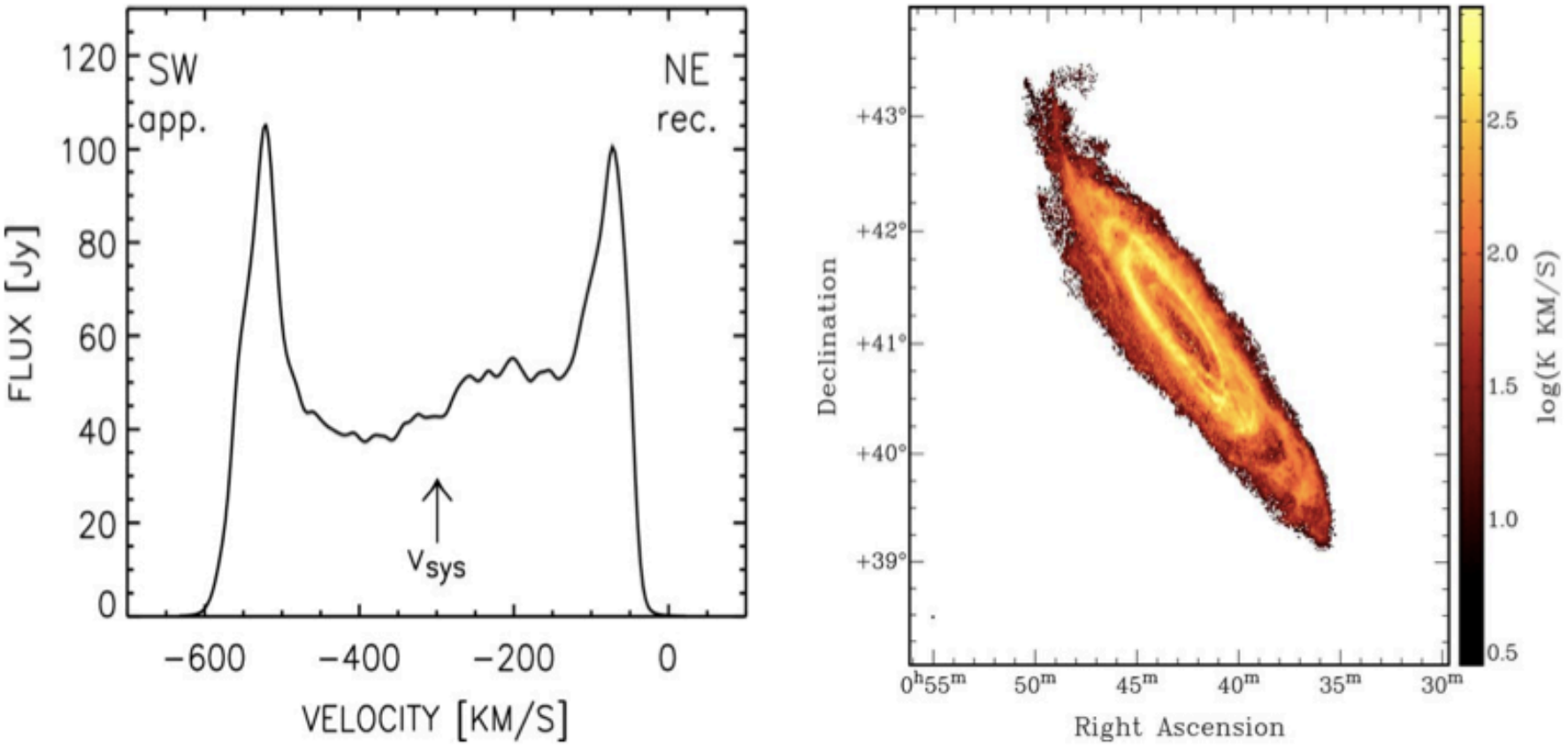

Figure 1.12: HI integrated profile (left panel), and total HI distribution of M 31 (right panel) from DRAO observations (Chemin et al., 2009).

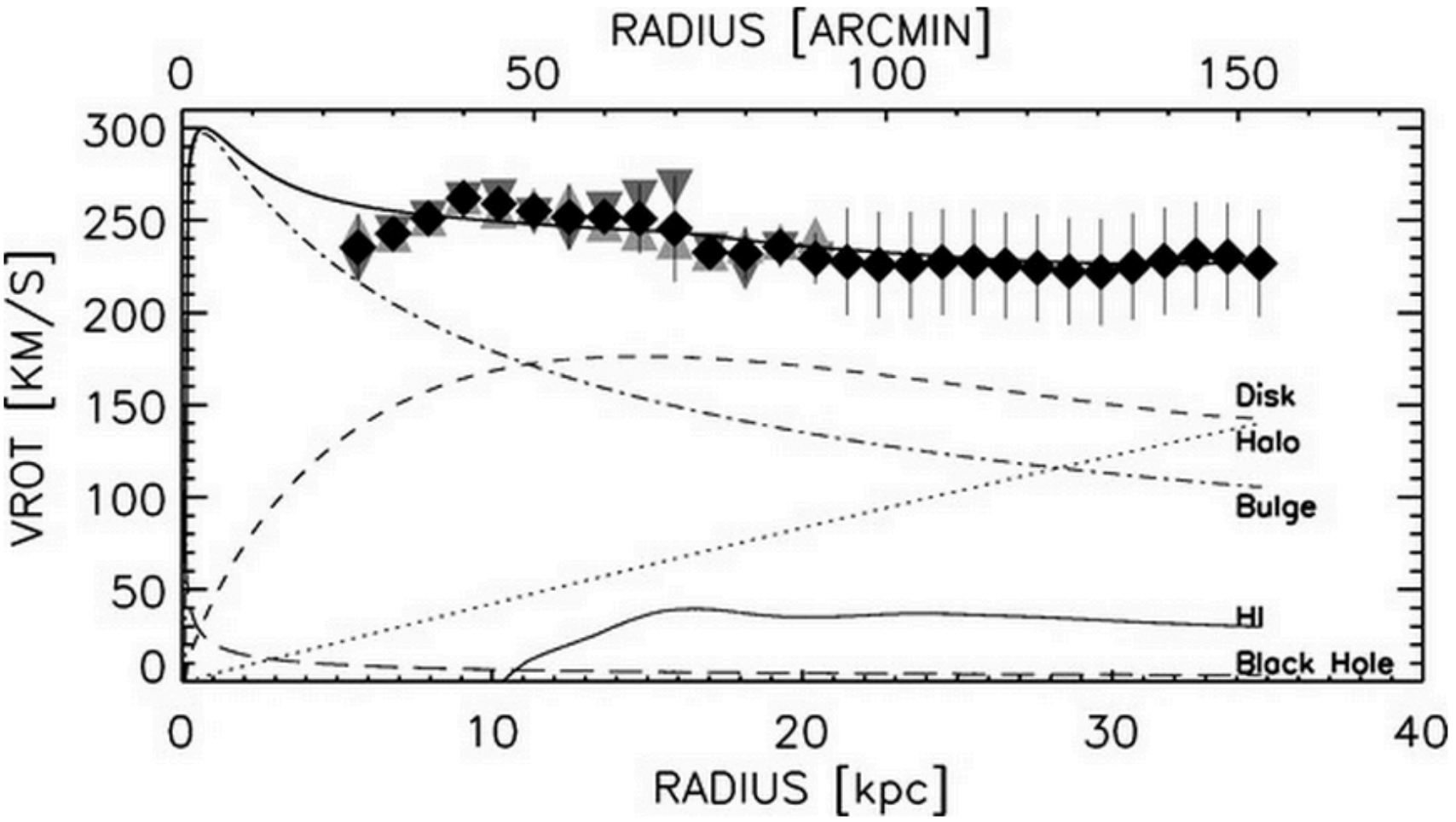
RADIUS [ARCMIN]
0
50
100
150
300
250
200
150
100
50
0
VROT [KM/S]
Disk
Halo
Bulge
HI
Black Hole
0
10
20
30
40
RADIUS [kpc]

Carignan+06

Fuel to Fireworks

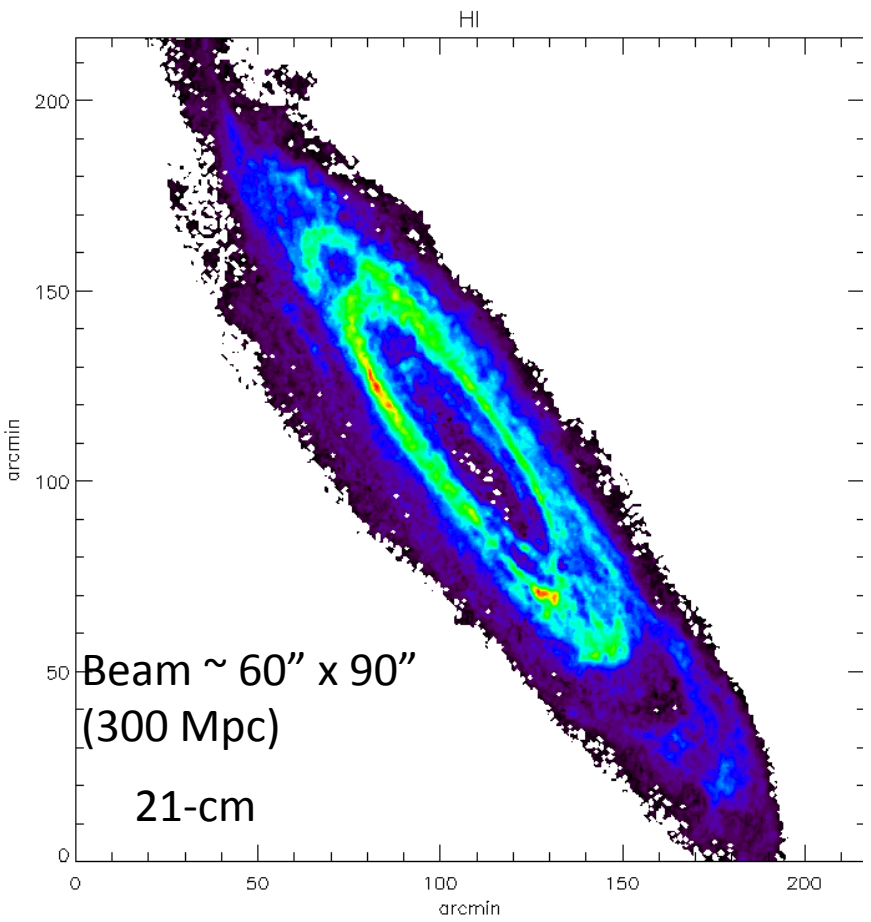

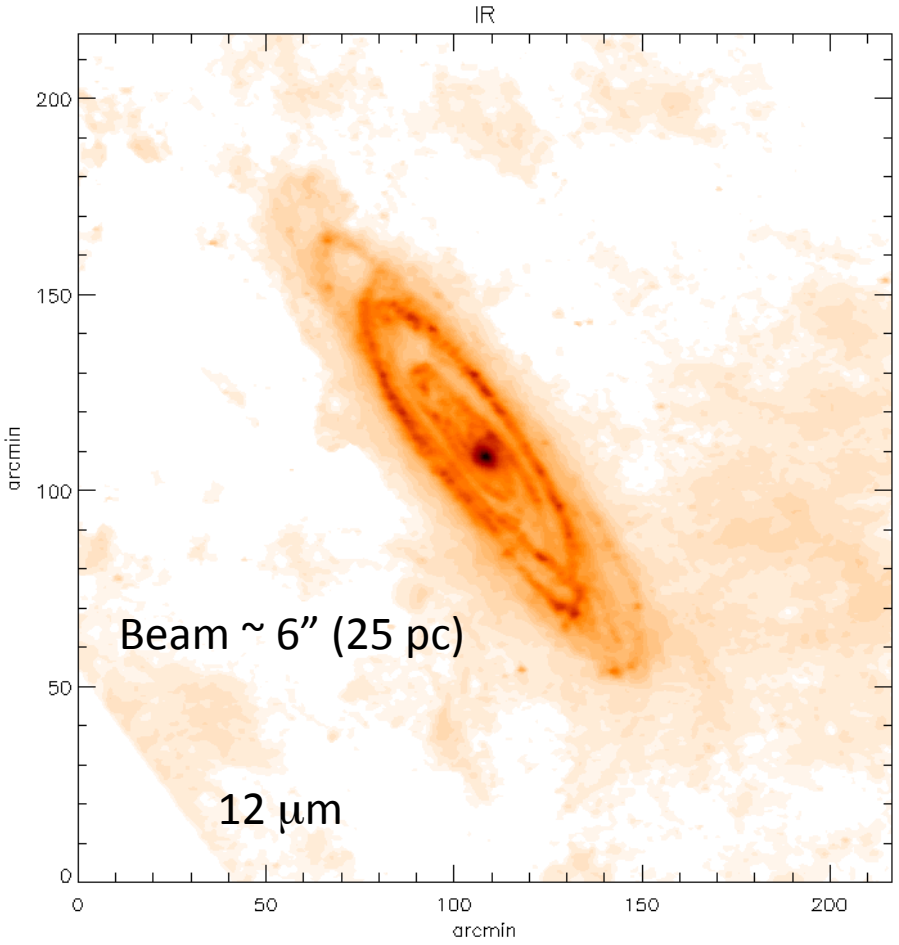

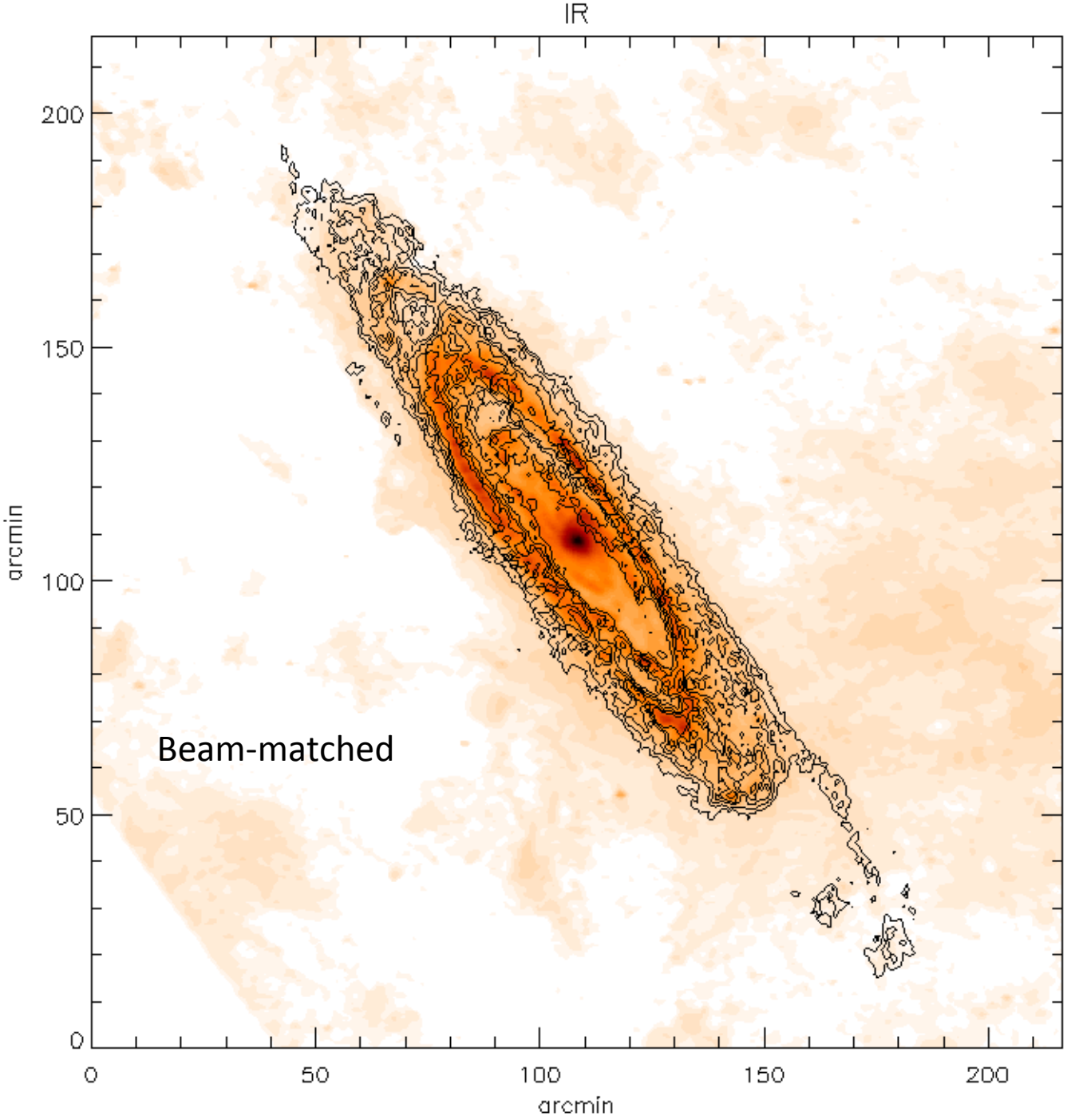
IR
200
150
100
50
0
arcmin
0
50
100
150
200
arcmin
Beam-matched

Multi-Phase Gas?

Column Densities

1.25e21 blue
1.75e21 green
2.25e21 red
3.00e21 violet

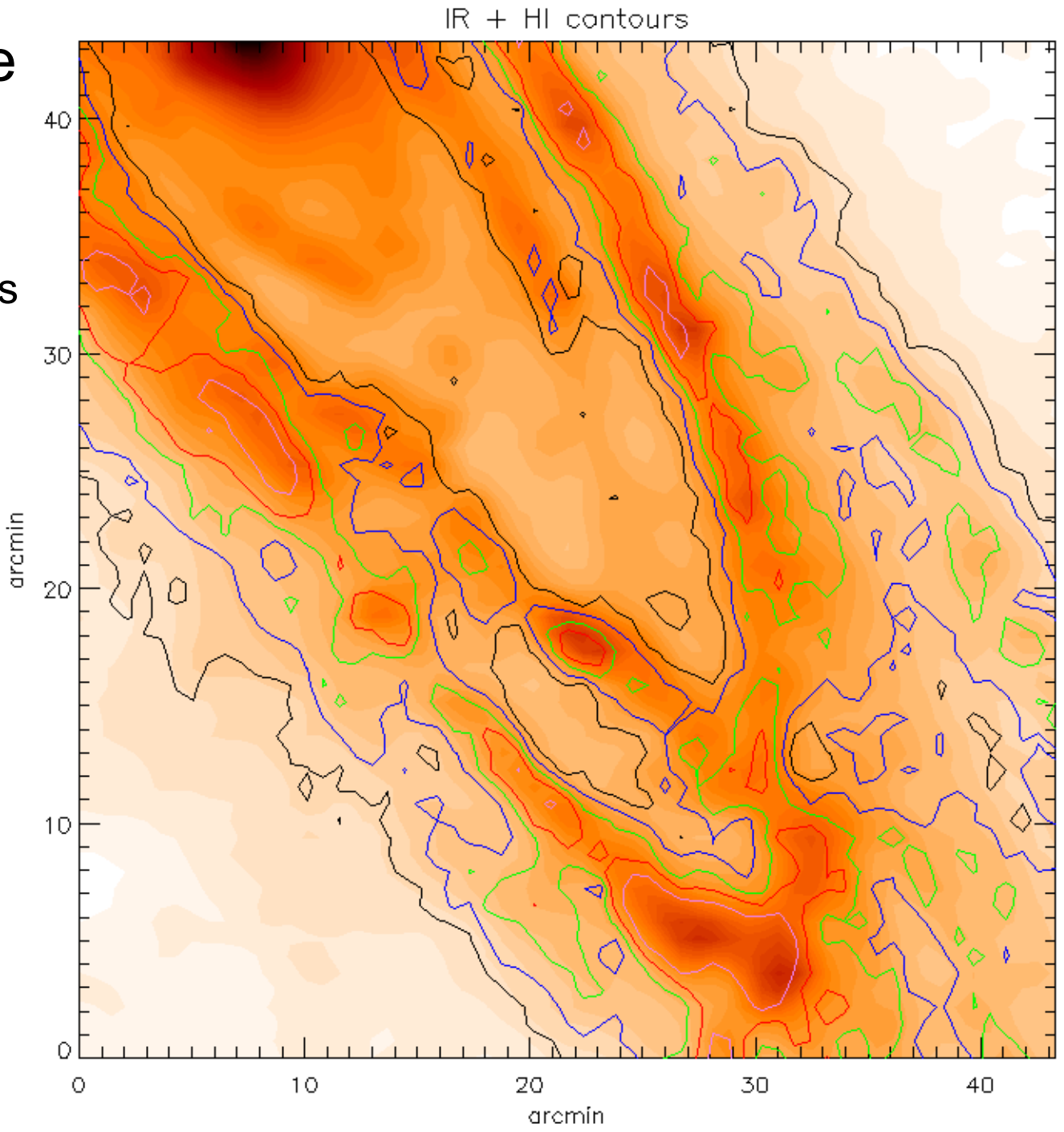

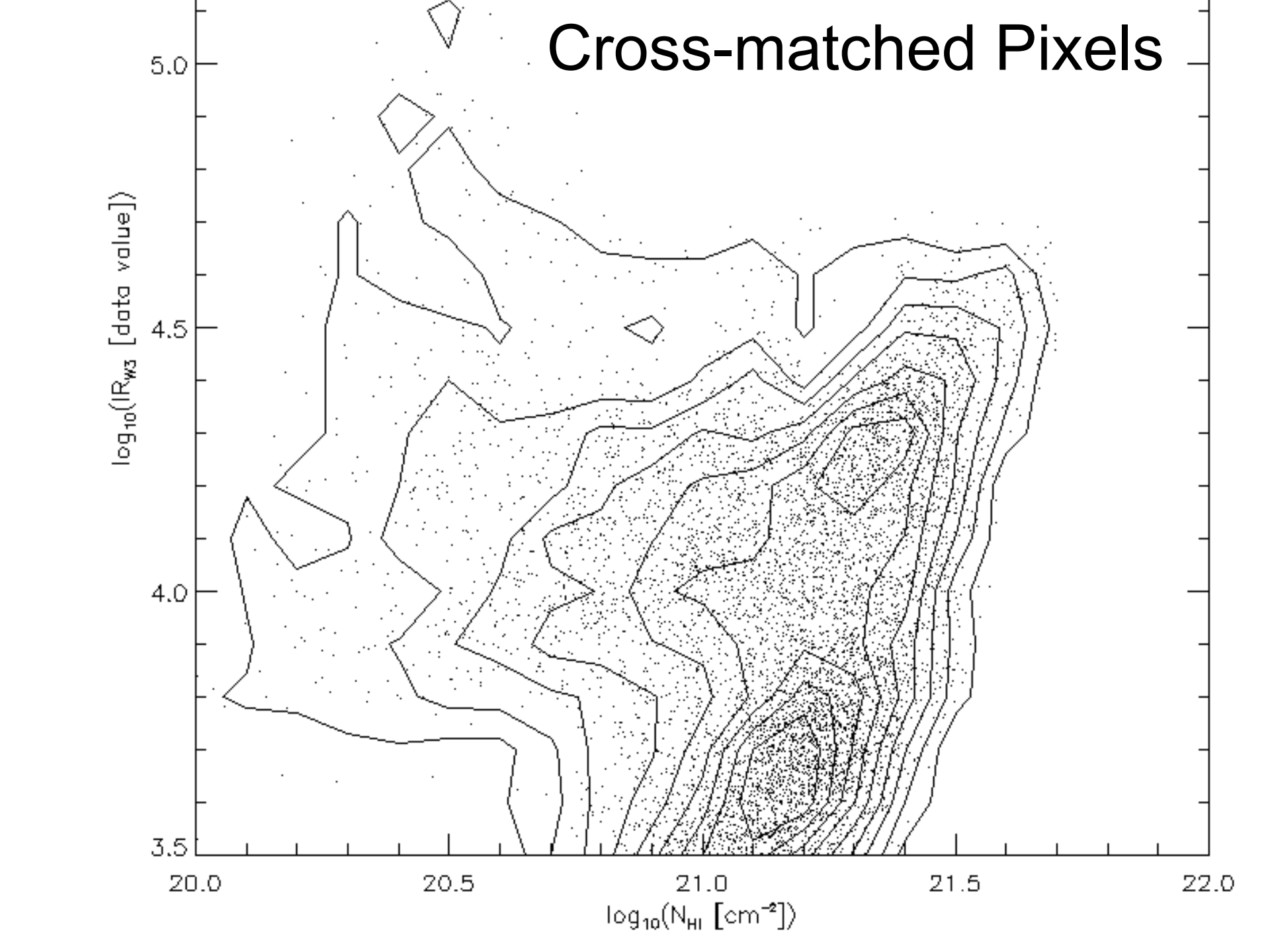
Cross-matched Pixels
5.0
4.5
4.0
3.5
20.0
20.5
21.0
21.5
22.0
log10(IRW3 [data value])
log10(NHI [cm-2])

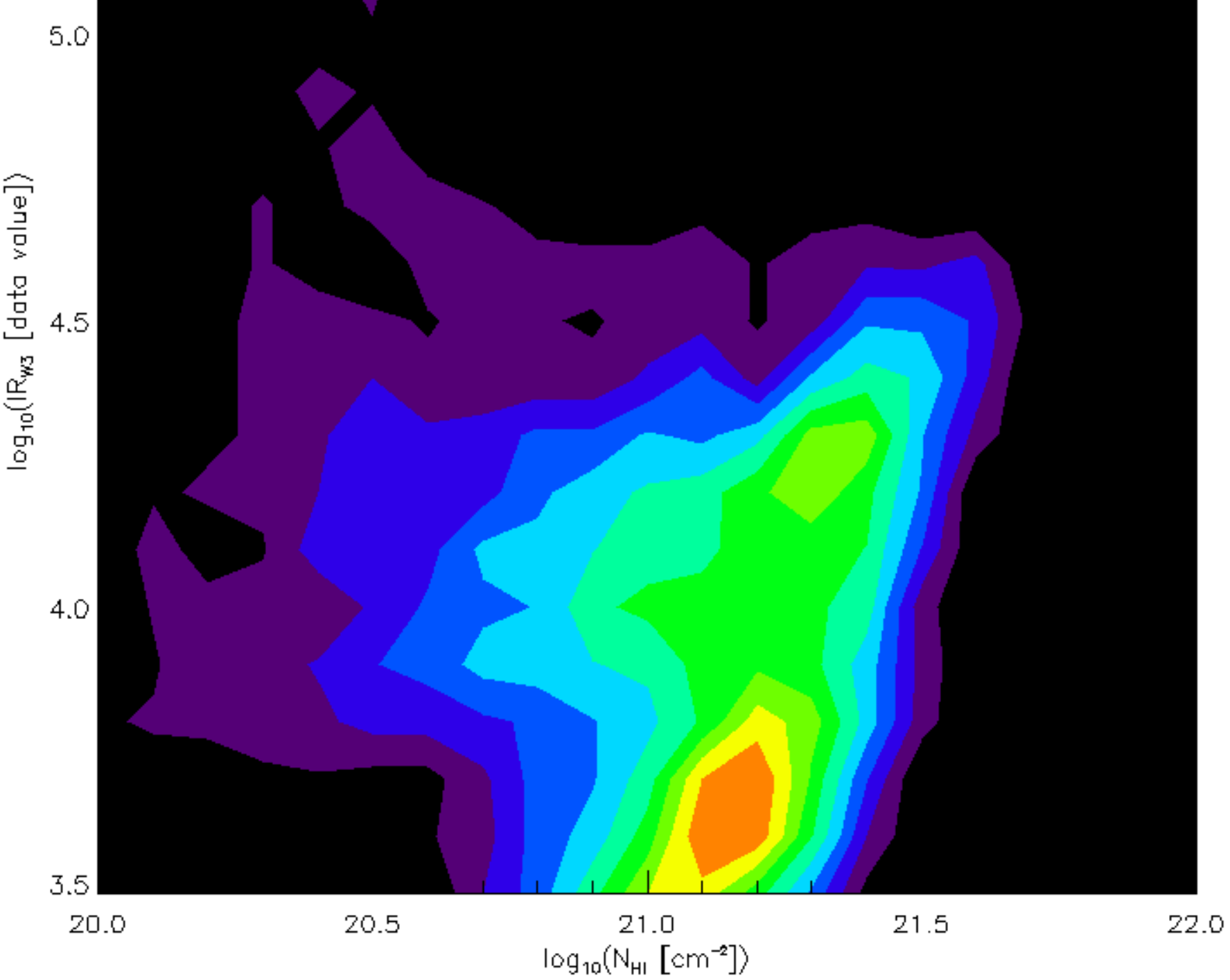
5.0
4.5
4.0
3.5
log10(IRW3 [data value])
20.0
20.5
21.0
21.5
22.0
log10(NHI [cm-2])

Arm vs intra-arm

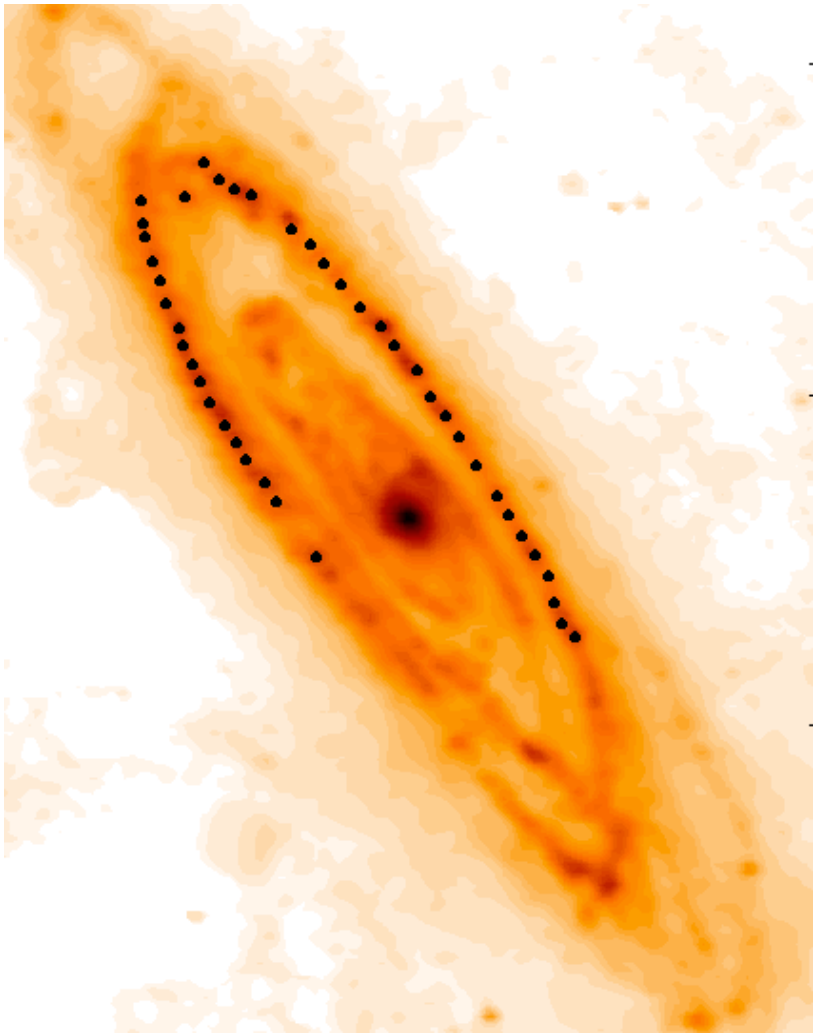

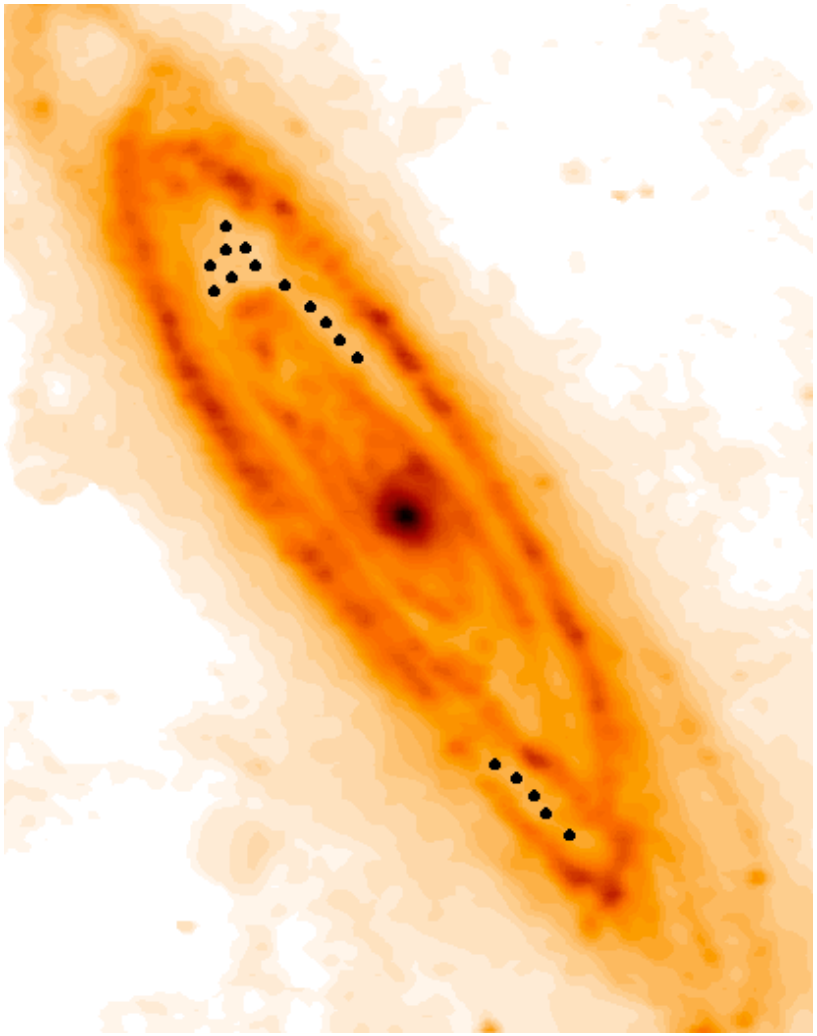

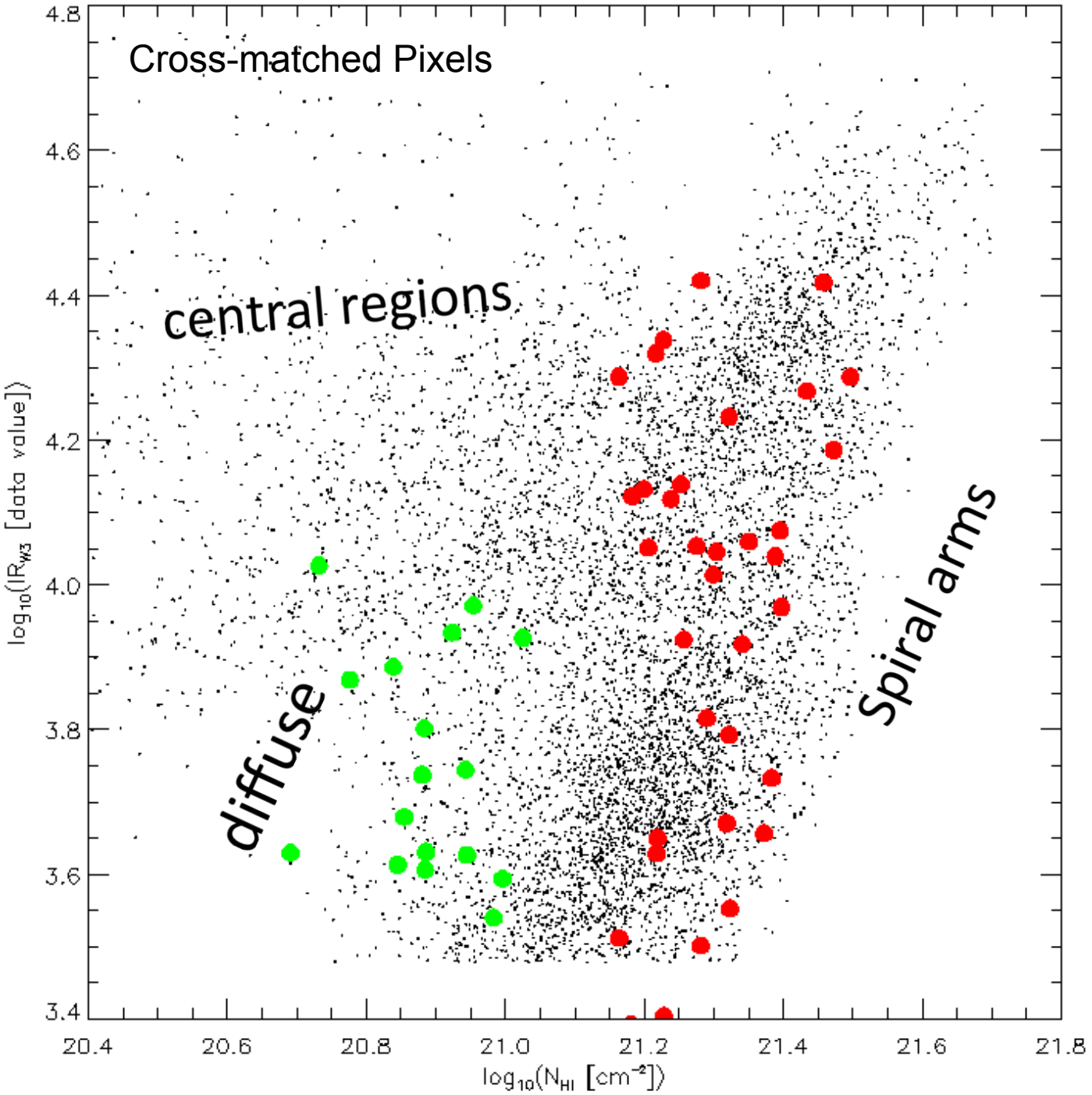
Cross-matched Pixels
central regions
diffuse
Spiral arms
4.8
4.6
4.4
4.2
4.0
3.8
3.6
3.4
20.4
20.6
20.8
21.0
21.2
21.4
21.6
21.8
log10(IRW3 [data value])
log10(NHI [cm-2])

Global Comparison

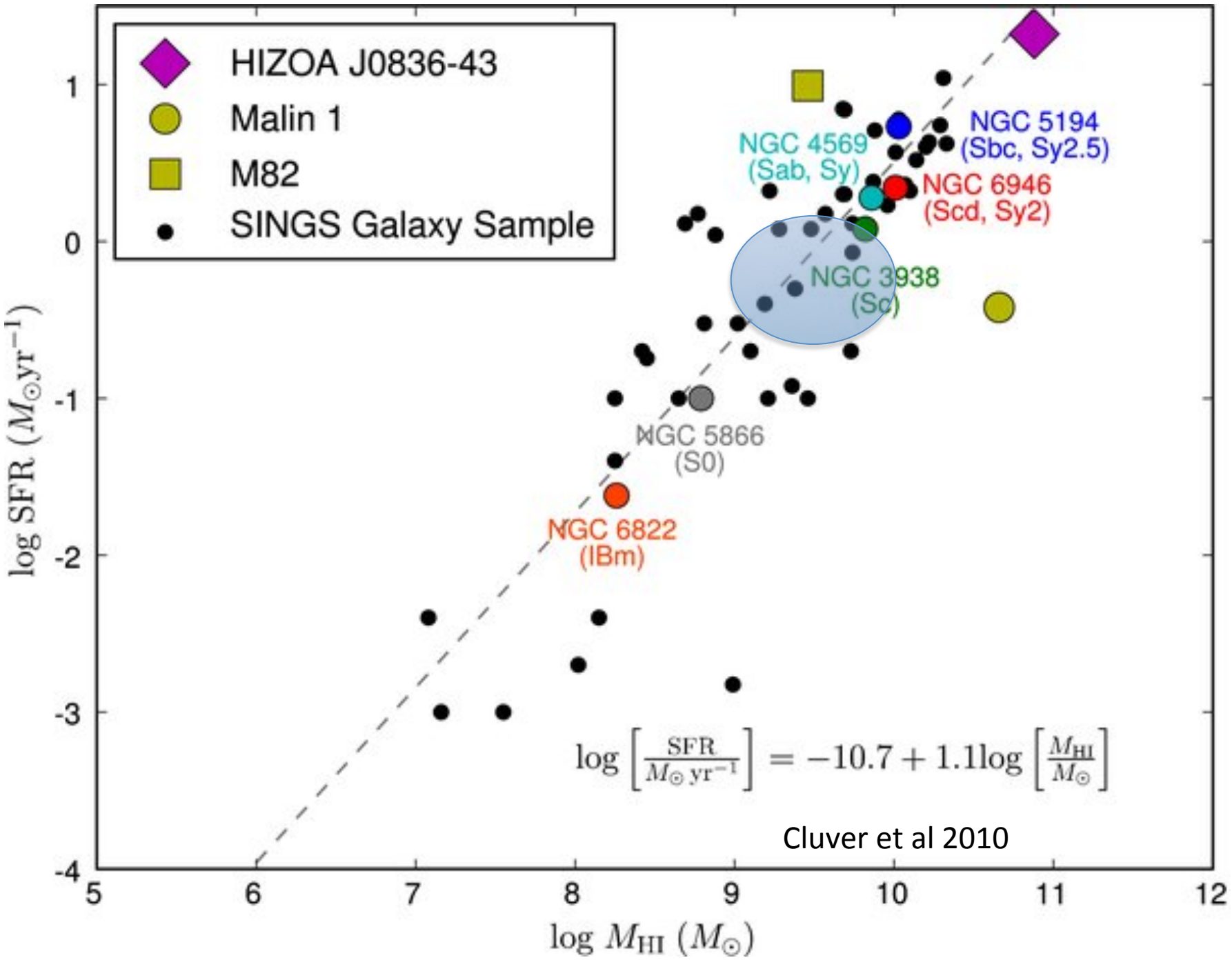
HIZOA J0836-43
Malin 1
M82
SINGS Galaxy Sample
NGC 5194
(Sbc, Sy2.5)
NGC 4569
(Sab, Sy)
NGC 6946
(Scd, Sy2)
NGC 3938
(Sc)
NGC 5866
(S0)
NGC 6822
(IBm)
$\log\left[\frac{\mathrm{SFR}}{M_\odot\,\mathrm{yr}^{-1}}\right] = -10.7 + 1.1\log\left[\frac{M_{\mathrm{HI}}}{M_\odot}\right]$
Cluver et al 2010
log SFR ($M_\odot$yr^{-1})
log M_{HI} ($M_\odot$)
1
0
-1
-2
-3
-4
5
6
7
8
9
10
11
12

Local Volume Results

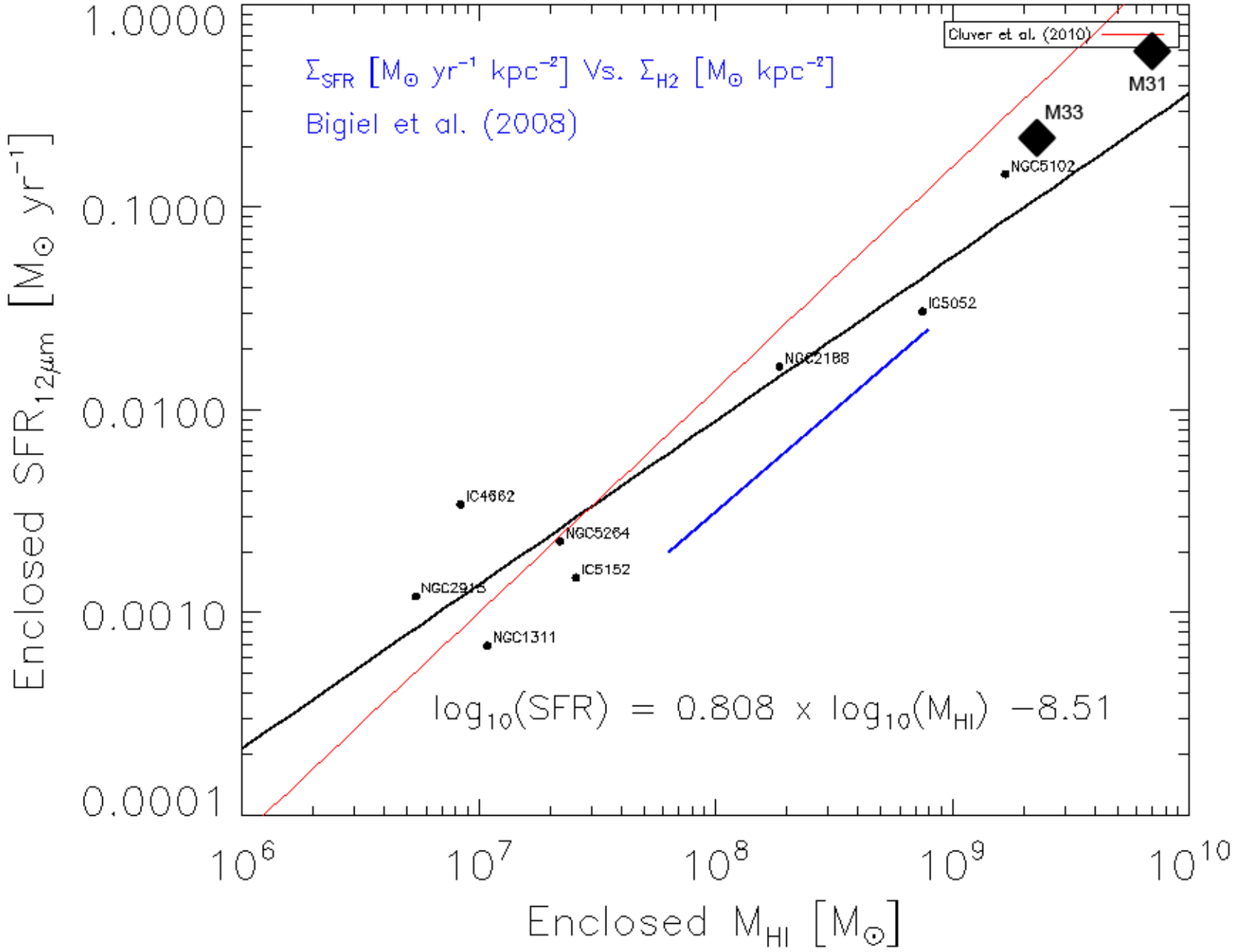

fini